Nuclear Engineering and Technology 55 (2023) 4395–4407

Contents lists available at ScienceDirect

Nuclear Engineering and Technology

journal homepage: www.elsevier.com/locate/net

Original Article

# Using a Lagrangian-Lagrangian approach for studying flow behavior inside a bubble column

YoungWoo Son [a], Cheol-O Ahn [b], SangHwan Lee [a,*]

[a] Department of Mechanical Engineering, Hanyang University, 222, Wangsimni-ro, Seongdong-gu, Seoul, 04763, Republic of Korea
[b] Metariver Technology Co. Ltd., C-716, SK-V1-GL-Metrocity, 128 Beobwon-ro, Songpa-gu, Seoul, 05854, Republic of Korea

ARTICLE INFO

*Keywords:*
Bubble column
Discrete bubble method (DBM)
Moving particle semi-implicit (MPS) method
Lagrangian-Lagrangian simulation
Volume fraction
Drag correlation

ABSTRACT

Bubble columns are widely encountered in several industries, especially in the field of nuclear safety. The Eulerian-Eulerian and the Eulerian-Lagrangian methods are commonly used to investigate bubble columns. Eulerian approaches require additional tasks such as strict volume conservation at the interface and a predefined well-structured grid. In contrast, the Lagrangian approach can be easily implemented. Hence, we introduce a fully Lagrangian approach for the simulation of bubble columns using the discrete bubble model (DBM) and moving particle semi-implicit (MPS) methods. Additionally, we propose a rigorous method to estimate the volume fraction accurately, and verified it through experimental data and analytical results. The MPS method was compared with the experimental data of Dambreak. The DBM was verified by analyzing the terminal velocity of a single bubble for each bubble size. It agreed with the analytical results for each of the four drag correlations. Additionally, the improved method for calculating the volume fraction showed agreement with the Ergun equation for the pressure drop in a packed bed. The implemented MPS-DBM was used to simulate the bubble column, and the results were compared with the experimental results. We demonstrated that the MPS-DBM was in quantitative agreement with the experimental data.

## 1. Introduction

Bubble columns are widely encountered in several industries, including chemical, biological, and nuclear. In particular, the hydrodynamics of a bubble column have become an increasingly important issue in nuclear reactor safety following the Fukushima accident. One of the most critical problems in the accident was the release of radioactive materials into the environment. To prevent corium from penetrating the barriers in the reactor cavity, it is necessary to study the bubble column generated by decay heat from hot corium [1].

When the corium falls into the coolant in the cavity, a bubble column is generated from the boiling coolant by decay heat from the corium. The bubble column induces not only effective heat exchange but also bubble-induced convection, which changes the surface area of the packed hot corium. In order to prevent reactor cavity erosion due to Molten Corium Concrete Interaction, it is necessary to evaluate the coolability of the packed bed [2–4]. The study of bubble-liquid hydrodynamics affecting the packed bed formation such as sloshing and leveling has been studied as one of the important phenomena for reactor design [1,5,6]. In this study, we focus on a bubble column flow as a proceeding study to understand the effect of it on the shape of a debris bed.

Kim et al. [1,7] conducted an experiment to find out about the internal and external structure of debris bed affected by rising bubble column flow. They generated bubbles by installing a gas injector below the cylinder and dropped particles into a cylindrical water tank. In case of the experiment for external shape of debris bed, air injection rate was controlled locally to simulate the generation of bubbles caused by the decay heat of corium particles. The results showed that upward bubble column flow affects particle settling trajectories, as well as their arrival location, resulting in the formation of a debris bed with a larger radius than under quiescent conditions, which is favorable for cooling [7]. The experiment for the internal shape of debris bed was conducted to determine the changes in radial and axial distribution in the particle bed under bubble column flow. The study showed the establishment of inhomogeneity in the internal structure of debris beds under realistic sedimentation conditions of natural convection induced by bubble column flow, and they also suggested the implications of such inhomogeneity on the debris bed coolability [1].

Konovalenko et al. [8] conducted experiments to provide validation data for the spreading of the debris particle in the pool by bubble column

* Corresponding author.
*E-mail address:* shlee@hanyang.ac.kr (S. Lee).

https://doi.org/10.1016/j.net.2023.08.018
Received 2 March 2023; Received in revised form 27 July 2023; Accepted 10 August 2023
Available online 12 August 2023

flow to develop codes and models for stable reactor design. The experiment addressed the influence on the gas flow rate, pool dimensions, particle density and size in a rectangular tank with a 2D slice geometry. As a result, the experimental data suggested that the gas injection rate, pool dimensions, and particle properties have a strong influence on debris bed formation [8].

The study of gas-liquid interactions has been carried out using either numerical simulations or experiments. Experimental research is difficult owing to the limited measurements and the absence of techniques to measure microscopic parameters [9]. Under these circumstances, computational fluid dynamics (CFD) is an important tool for the study of spatial and temporal features of bubble behavior, although there are several difficulties, such as unstable interface tracking, interacting forces, and discontinuous density fields with a high-density ratio.

In the past decade, several studies have provided detailed insight into the dynamics of the bubble column flow through two types of numerical modeling. One is Eulerian-Eulerian (EE) model, which treats liquid and bubbles as continua. The number of bubbles depending on the calculation cells are presented as volume fractions, and a volume-averaged mass and momentum conservation equation is adopted to describe the movement of the bubble column. To resolve discontinuities in the interfacial properties, several methods have been used for tracking the interface motion, such as the volume-of-fluid (VOF), front-tracking (FT), and level-set (LS) methods. These approaches are generally used to study bubble columns. However, there are some weak points, such as computational expense and lack of mass conservation [10,11]. In the Eulerian-Lagrangian (EL) model, continuous phases are modeled using the Eulerian method, and the dispersed bubble is directly tracked using Newtonian equations of motion without an additional tracking method [12]. Therefore, the additional effect of the interaction between bubble-bubble and bubble-liquid can be directly considered, such as mass transfer [12,13], coalescence, and breakup [9,14].

Most studies on the numerical investigation of bubble columns employ the Eulerian method for continuous phase modeling. However, the grid-based Eulerian approach still has shortcomings in simulating bubble columns. One of the disadvantages of the Eulerian approach is that prior investigation is required for the optimization of the mesh owing to its dependency on the mesh quality [15,16]. In addition, it is difficult to satisfy strict volume conservation and represent dynamic movements at the free surface and interface; therefore, additional work is required [9,17]. In this study, we propose a Lagrangian-Lagrangian (LL) approach which employs continuous phase modeling to resolve the above problems.

A Lagrangian-Lagrangian coupling method has been applied to simulate multiphase flow. In case of liquid-solid interaction, the Moving particle semi-implicit (MPS) method or Smoothed particle hydrodynamics (SPH) method has been used for continuous phase and, the Discrete element method (DEM) has been used for discrete phase. Based on SPH-DEM coupling, Sun et al. [18] simulated a solid-liquid dam break and a quasi-steady flow in a rotating cylindrical tank and compared it through experimental data. M. Robinson et al. [19] simulated single and multiple particle sedimentation based on SPH-DEM coupling and compared the results with analytic solution and experimental results. Neethling and Barker [20]. simulated various applications related to the minerals processing system using SPH-DEM. Jo et al. [2] simulated the vapor-driven 3-phase leveling behavior of solid debris particles based on SPH and compared the results with experiments. In addition, Harada et al. [21–23] and Tazaki et al. [24] simulated particle size sorting processing, sediment transport, and ripple formation process in the coastal area through MPS-DEM coupling, and validation experiments were performed and compared with the results.

In this paper, the MPS method was utilized for continuous phase analysis, which was proposed by Koshizuka et al. [25–27]. Unlike Eulerian-based VOF, in MPS, each representative particle with physical properties moves and interacts with neighboring particles within a pre-defined range [25]. Therefore, the MPS method has been reported to be effective for simulating complicated interfacial flows without any additional effort to calculate transport equation [21,27–31]. For dispersed phase analysis, the discrete bubble model (DBM) was utilized. In the DBM, the bubbles are represented as dispersed elements and traced along the trajectory by their equation of motion. As a particle is represented as a single bubble, the DBM method has been used to simulate mesoscale bubble–liquid interactions [9,11–14,32]. In this study, we propose a MPS-DBM to simulate the bubble column flow with a high gas holdup. The proposed MPS-DBM cannot consider the detailed motion and deformable interface of a bubble, unlike a direct numerical simulation that calculates all the flow around a deformable bubble in a low gas holdup condition [15]. However, we apply drag correlations to consider effects of bubble shape and successfully present the bubble swarm behavior, in which a large number of bubbles interact in a liquid (high gas holdup). The drag correlation has been widely used for an EE and EL coupling in many literatures [12,33–36].

To achieve high computational efficiency, the fully Lagrangian approach was parallelized using a single graphics processing unit (GPU). GPU computing is suitable for the particle-based Lagrangian method for high-throughput computation [37].

## 2. Governing equations

In this study, a meshless approach that does not require a grid is implemented by a full Lagrangian-Lagrangian approach. For this purpose, the MPS method and DBM are used to analyze the liquid and gas phases, respectively.

### 2.1. Liquid phase

For the liquid phase analysis, the MPS method proposed by Koshizuka was used. MPS is a Lagrangian analysis technique that is widely used together with SPH. To ensure liquid incompressibility and stable simulation, it adopts a semi-implicit algorithm and calculates the pressure field by solving the pressure Poisson equation (PPE). If the polygonal wall boundary model is used, additional work, such as the generation of wall particles, is not required to implement the wall boundary condition.

For incompressible flow, the mass and momentum conservation equation are defined as follows.

$$\frac{D\rho}{Dt} = -\rho\nabla \bullet \vec{u} \tag{1}$$

$$\frac{D\vec{u}}{Dt} = -\frac{1}{\rho}\nabla p + \nu\nabla^2\vec{u} + \vec{g} \tag{2}$$

where $\vec{u}$ is the velocity vector of the liquid, $\rho$ is the density of the liquid, $p$ is the pressure, $\nu$ is the kinematic viscosity of the liquid, and $\vec{g}$ is the gravitational acceleration. According to this method, a particle interacts with neighboring particles based on the weight function as follows:

$$w\left(\left|\vec{r}_{ij}\right|\right) = \begin{cases} \dfrac{r_e}{\left|\vec{r}_{ij}\right|} - 1, & 0 < \left|\vec{r}_{ij}\right| < r_e \\ 0, & r_e \le \left|\vec{r}_{ij}\right| \end{cases} \tag{3}$$

where $r_e$ is the effective radius. Usually, when the initial particle-to-particle spacing is $l_0$, $r_e$ is 3.1 $l_0$. The number density of particles can be obtained from the neighboring particles within a distance $r_e$.

$$n^0 = \sum_{i \neq j} w\left(\left|\vec{r}_{ij}\right|\right) \tag{4}$$

The following PPE is used to calculate pressure.

$$\langle \nabla^2 p \rangle_i^{k+1} = -\frac{\rho^0}{(\Delta t)^2}\frac{n_i^{k+1/2} - n^0}{n^0} \tag{5}$$

The above expression can be written as follows according to the Laplacian operator defined in MPS:

$$\frac{2d}{\lambda n^0}\sum_{i\neq j}\left(p_j^{k+1} - p_i^{k+1}\right) w\left(\left|\vec{r}_{ij}\right|\right) = -\frac{\rho^0}{(\Delta t)^2}\frac{n_i^{k+1/2} - n^0}{n^0} \tag{6}$$

where $d$ is a number corresponding to the dimension. $n^0$ is the reference particle number density, which is determined by Eq. (4) from the initial arrangement of the liquid particles. The $\lambda$ of Eq. (6) is also defined as follows from the initial arrangement of the liquid particles.

$$\lambda = \frac{\sum_{i\neq j}\left|\vec{r}_{ij}\right|^2 w\left(\left|\vec{r}_{ij}\right|\right)}{\sum_{i\neq j} w\left(\left|\vec{r}_{ij}\right|\right)} \tag{7}$$

The conventional MPS method described thus far often suffers from problems in terms of accuracy and stability. To solve this problem of the MPS method, Duan et al. [29] used a corrective matrix for the MPS kernel and extended it to the multiphase MPS-continuous acceleration (MMPS-CA) method.

The corrective matrix is defined as follows.

$$\boldsymbol{C}_i^{-1} = \frac{d}{n^0}\begin{bmatrix} \sum_{i\neq j}\frac{x_{ij}^2}{\left|\vec{r}_{ij}\right|^2} w\left(\left|\vec{r}_{ij}\right|\right) & \sum_{i\neq j}\frac{x_{ij}y_{ij}}{\left|\vec{r}_{ij}\right|^2} w\left(\left|\vec{r}_{ij}\right|\right) & \sum_{i\neq j}\frac{x_{ij}z_{ij}}{\left|\vec{r}_{ij}\right|^2} w\left(\left|\vec{r}_{ij}\right|\right) \\ \sum_{i\neq j}\frac{y_{ij}x_{ij}}{\left|\vec{r}_{ij}\right|^2} w\left(\left|\vec{r}_{ij}\right|\right) & \sum_{i\neq j}\frac{y_{ij}^2}{\left|\vec{r}_{ij}\right|^2} w\left(\left|\vec{r}_{ij}\right|\right) & \sum_{i\neq j}\frac{y_{ij}z_{ij}}{\left|\vec{r}_{ij}\right|^2} w\left(\left|\vec{r}_{ij}\right|\right) \\ \sum_{i\neq j}\frac{z_{ij}x_{ij}}{\left|\vec{r}_{ij}\right|^2} w\left(\left|\vec{r}_{ij}\right|\right) & \sum_{i\neq j}\frac{z_{ij}y_{ij}}{\left|\vec{r}_{ij}\right|^2} w\left(\left|\vec{r}_{ij}\right|\right) & \sum_{i\neq j}\frac{z_{ij}^2}{\left|\vec{r}_{ij}\right|^2} w\left(\left|\vec{r}_{ij}\right|\right) \end{bmatrix} \tag{8}$$

$$\boldsymbol{L}_i = \frac{2d}{n^0\lambda}\left[\sum_{i\neq j} x_{ij} w\left(\vec{r}_{ij}\right) \quad \sum_{i\neq j} y_{ij} w\left(\vec{r}_{ij}\right) \quad \sum_{i\neq j} z_{ij} w\left(\vec{r}_{ij}\right)\right] \tag{9}$$

The matrix of Eq. (8), and the vector of Eq. (9) must be calculated for all particles. The 1st term of momentum in Eq. (2), expressed by MMPS-CA, is as follows:

$$\left\langle \frac{1}{\rho}\nabla p \right\rangle_i = \frac{d}{n^0}\sum_{i\neq j}\left\{\left(\frac{2}{\rho_i + \rho_j}\right)\left(p_j^{k+1} - p_i^{k+1}\right)\frac{\boldsymbol{C}_i\vec{r}_{ij}}{\left|\vec{r}_{ij}\right|^2} w\left(\left|\vec{r}_{ij}\right|\right)\right\} \tag{10}$$

the 2nd term of the momentum in Eq. (2), expressed by MMPS-CA, is as follows:

$$\left\langle \frac{1}{\rho}\nabla\cdot(\mu\nabla\vec{u}) \right\rangle_i = \frac{d}{n^0}\sum_{i\neq j}\left\{\left(\frac{2\mu_i\mu_j}{\mu_i + \mu_j}\right)\left(\frac{2}{\rho_i + \rho_j}\right)\vec{u}_{ij}\left(\frac{2}{\lambda} - \frac{\boldsymbol{L}_i\boldsymbol{C}_i\vec{r}_{ij}}{\left|\vec{r}_{ij}\right|^2}\right) w\left(\left|\vec{r}_{ij}\right|\right)\right\} \tag{11}$$

For turbulence modeling, the Subparticle-scale (SPS) turbulence model proposed by Gotoh et al. [38] and the wall model proposed by Arai et al. [39] were used.

### 2.2. Gas phase

The DBM is implemented to describe the behavior of bubbles in liquids. This model was first introduced by Delnoij et al. [40]. The original DBM can be applied to the dispersed phases targeting relatively small spherical bubbles that do not coalesce or break up, and where the bubble size is considered to be constant. Some researchers have attempted bubble coalescence and break-up; however, this study did not consider them.

Each bubble is tracked by the following equation of motion.

$$\rho_B V_B\frac{d\vec{u}_B}{dt} = \vec{F}_B \tag{12}$$

Here, $\rho_B$, $V_B$, $\vec{u}_B$ and $\vec{F}_B$ are the gas phase density, volume of the bubble, velocity of the bubble, and total force acting on the bubble, respectively.

$\vec{F}_B$ is computed as follows.

$$\vec{F}_B = \vec{F}_G + \vec{F}_D + \vec{F}_L + \vec{F}_P + \vec{F}_W + \vec{F}_V + \vec{F}_T \tag{13}$$

where $\vec{F}_G$, $\vec{F}_D$, $\vec{F}_L$, $\vec{F}_P$, $\vec{F}_W$, $\vec{F}_V$ and $\vec{F}_T$ are the forces owing to gravity, drag, lift, pressure gradient force, wall effect force, virtual mass force, and turbulent dispersion force, respectively. These forces are assumed to be independent and uncoupled from each other.

The force acting on a bubble, due to gravity, is determined as follows.

$$\vec{F}_G = V_B\rho_B\vec{g} \tag{14}$$

The drag force is generated by the pressure distribution around the bubble and shear stress.

$$\vec{F}_D = \frac{1}{8}C_D\rho_L\pi d_B^2\left|\vec{u}_B - \vec{u}_L\right|\left(\vec{u}_B - \vec{u}_L\right) \tag{15}$$

where $C_D$ is the drag coefficient, $d_B$ is the diameter of the bubble, and $\vec{u}_L$ is the velocity of the liquid.

The Reynolds number of the bubble is defined as follows.

$$R_{EB} = \frac{\rho_L\left|\vec{u}_B - \vec{u}_L\right|d_B}{\mu_L} \tag{16}$$

When expressing the surface tension coefficient as $\sigma$, the Eötvös number ($E_O$), which is the ratio of gravitational forces to surface tension forces, is determined as follows:

$$E_O = \frac{\vec{g}(\rho_L - \rho_B)d_B^2}{\sigma} \tag{17}$$

The drag coefficient $C_D$ is strongly dependent on the Reynolds number ($R_{EB}$) of the bubble and $E_O$.

The drag coefficient correlation proposed by Ishii and Zuber (IZ) [35] is as follows:

$$C_{D\infty,\mathrm{IZ}} = max\left\{C_{D,\mathrm{sphere}}, min\left(C_{D,\mathrm{ellipse}}, C_{D,\mathrm{cap}}\right)\right\}$$

where,

$$\begin{cases} C_{D,\mathrm{sphere}} = \dfrac{24}{R_{EB}}\left(1 + 0.1R_{EB}^{0.75}\right) \\ C_{D,\mathrm{ellipse}} = \dfrac{2}{3}\sqrt{E_O} \\ C_{D,\mathrm{cap}} = \dfrac{8}{3} \end{cases} \tag{18}$$

Tomiyama proposed the following three drag coefficient correlations according to the degree of contamination [35].

$$\text{for a pure system } C_{D\infty,\mathrm{TP}} = max\left[min\left\{\frac{16}{R_{EB}}\left(1 + 0.15R_{EB}^{0.687}\right), \frac{48}{R_{EB}}\right\}, \frac{8}{3}\frac{E_O}{E_O + 4}\right] \tag{19}$$

for a slightly contaminated system $C_{D\infty,\mathrm{TS}} = max\left[min\left\{\frac{24}{R_{EB}}\left(1+0.15R_{EB}^{0.687}\right), \frac{72}{R_{EB}}\right\}, \frac{8}{3}\frac{E_O}{E_O+4}\right]$ (20)

for a contaminated system $C_{D\infty,\mathrm{TC}} = max\left\{\frac{24}{R_{EB}}\left(1+0.15R_{EB}^{0.687}\right), \frac{8}{3}\frac{E_O}{E_O+4}\right\}$ (21)

Eqs. 18–21 all depict the expressions for the drag coefficients for a single bubble, and when $\varepsilon_B$ is the gas volume fraction, the drag coefficient due to the swarm effect of the bubble can be obtained as follows [41]:

$$C_D = C_{D\infty}\left(e^{3.64\varepsilon_B} + \varepsilon_B^{0.864}\right) \quad (22)$$

A bubble rising in a nonuniform velocity field receives a lift force owing to the relative velocity between the liquids and the vorticity in the liquid flow field as follows:

$$\vec{F}_L = \rho_L V_B C_L\left(\vec{u}_L - \vec{u}_B\right) \times \nabla \times \vec{u}_L \quad (23)$$

Here, $C_L$ is the lift coefficient, and a correlation dependent on the Eötvös number was developed by Tomiyama et al. [42].

$$C_L = \begin{cases} min\{0.288\tanh(0.121R_{EB}), f(E_{OH})\} & E_{OH} < 4 \\ f(E_{OH}) & 4 \le E_{OH} < 10 \\ -0.27 & 10 \le E_{OH} \end{cases}$$

where

$$f(E_{OH}) = 0.00105E_{OH}^3 - 0.0159E_{OH}^2 - 0.0204E_{OH} + 0.474$$

$$E_{OH} = E_O\left(1+0.163E_O^{0.757}\right)^{2/3} \quad (24)$$

The pressure gradient force is caused by the uneven distribution of number density around the particle, which pushes the bubble out of the high-pressure region. This force is important when large pressure gradients exist or when the density difference between the two phases is large.

$$\vec{F}_P = -V_B\nabla p \quad (25)$$

The bubble near the wall is subjected to a force called the wall force, and this force exerts the effect of pushing the bubble away from the wall. In this study, the correlation by Tomiyama et al. [42] is used.

$$\vec{F}_W = \left(\frac{2\rho_L V_B}{d_B}\right)\left(\frac{d_B}{2y}\right)^2 C_W\left|\left(\vec{u}_L - \vec{u}_B\right)\vec{k}\right|^2 \vec{n}_W \quad (26)$$

$$C_W = \begin{cases} e^{-0.933E_O+1.79} & 1 \le E_O < 5 \\ 0.007E_O + 0.04 & 5 \le E_O < 33 \end{cases} \quad (27)$$

where $y$ is the shortest distance from the wall to the center of the bubble, $\vec{k}$ is the unit vector pointing upward in the vertical direction, and $\vec{n}_W$ is the wall normal vector. This wall force model has been implemented for a two-phase flow simulation, and similar models have been studied by Hosokawa et al. [43] and Rzehak et al. [44].

When a bubble is accelerated, a certain amount of liquid must also be set into motion. This force is called the virtual mass force or the added mass force.

$$\vec{F}_V = \varepsilon_B\rho_L C_V\left(\frac{D\vec{u}_L}{Dt} - \frac{D\vec{u}_B}{Dt}\right) \quad (28)$$

$D/Dt$ is a substantial derivative and the virtual mass force coefficient $C_V$ is 0.5. This force becomes more important as the density difference between the two phases increases [35].

The turbulent dispersion force causes the bubbles inside the turbulent flow field of the liquid to move from the high-density to the low-density side owing to the influence of turbulent fluctuations. In this study, the model proposed by Burns et al. [45] is used.

$$\vec{F}_T = -\frac{3}{4}C_D\frac{\varepsilon_B}{d_B}\left|\vec{u}_L - \vec{u}_B\right|\frac{\mu_L^{\mathrm{turb}}}{\sigma_{\mathrm{TD}}}\left(\frac{1}{\varepsilon_L} + \frac{1}{\varepsilon_B}\right)\nabla\varepsilon_B \quad (29)$$

Here, $\mu_L^{\mathrm{turb}}$ is the turbulent viscosity, $\sigma_{\mathrm{TD}}$ is the turbulent bubble Schmidt number (0.9), and $\varepsilon_L$ is the volume fraction of the liquid.

A nonlinear viscoelastic collision model that was proposed by Tsuji

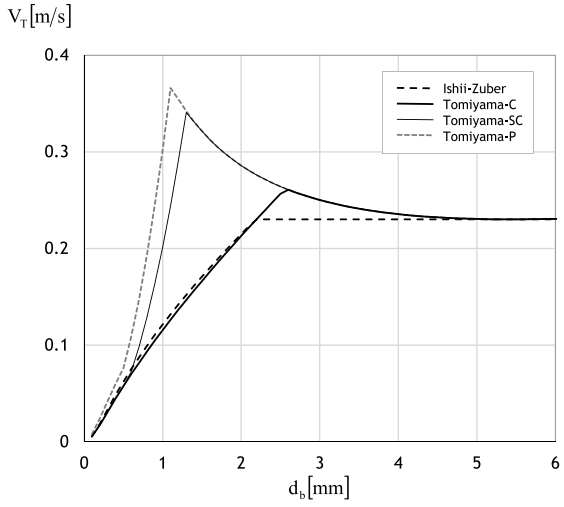


**Fig. 1.** Bubble terminal rising velocity of a single bubble depends on bubble diameters.

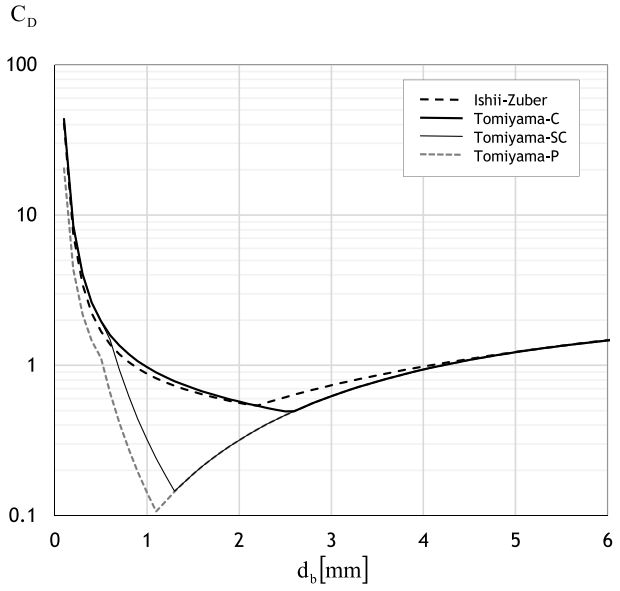


**Fig. 2.** Drag coefficient of a single bubble depends on bubble diameters.

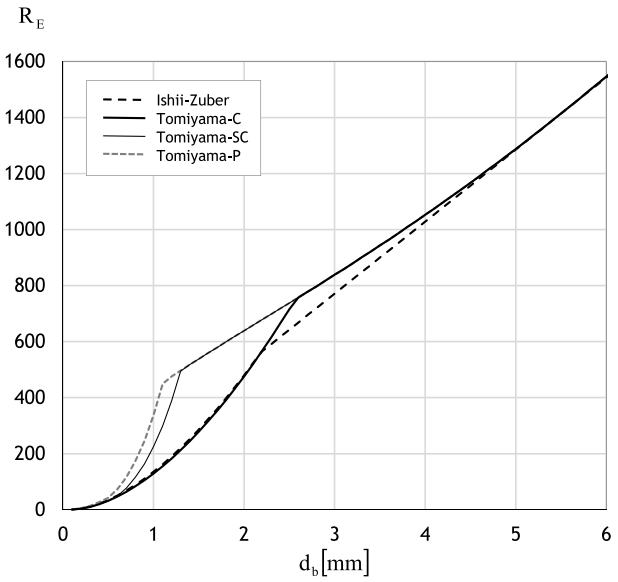


**Fig. 3.** The Reynolds number of a single bubble depends on bubble diameters.

et al. [46] was used to calculate the bubble-to-bubble contact force. Considering a single bubble existing in a quiescent liquid, the rising velocity is determined when the gravity, pressure gradient force, and drag force are in equilibrium.

$$(\rho_B-\rho_L)\vec{g}\frac{\pi d_B^3}{6}=\frac{\rho_L}{2}C_D\frac{\pi d_B^2}{4}\left|\vec{v}_{BT}\right|\vec{v}_{BT} \tag{30}$$

here, $\vec{v}_{BT}$ is the terminal rising velocity of the bubble.

$$\vec{v}_{BT}=\left\{\frac{4d_B(\rho_L-\rho_B)g}{3\rho_L C_D}\right\}^{1/2} \tag{31}$$

Stokes (1880), Davies and Taylor (1950), Haberman and Morton (1956), Mendelson (1967), Jamialahmadi et al. (1994), and Tomiyama et al. (1998, 2002) tried to establish the drag coefficient correlation using Eq. (31) by measuring the terminal rising velocity of a single bubble.

Fig. 1 shows the result of calculating the terminal rising velocity of a single bubble according to the diameter of the bubble using Eqs. (31) and (18-21).

The drag coefficient and Reynolds number obtained at convergence to the terminal rising velocity are shown in Figs. 2 and 3, respectively.

There are several interesting points in Figs. 1 and 2.

First, in Tomiyama contaminated (Tomiyama-C) model and Tomiyama slightly contaminated (Tomiyama-SC) model, in the case of a bubble diameter of approximately 1.2 mm, the bubble has the lowest drag coefficient, so it has the maximum terminal rising velocity. In all the four correlations used in this study, there is a point where the drag coefficient is minimized in the area with a bubble diameter of 1–3 mm. The point at which the drag coefficient is minimized is closely related to the degree of contamination of the liquid.

Second, even if the diameter of the bubble increases, the terminal rising velocity converges to a constant value when it is more than approximately 4 mm. As the diameter increases, the drag coefficient also increases gradually. It has almost the same terminal rising velocity as the drag, even if the buoyancy increases with the diameter of the bubble.

Third, the drag coefficients of Tomiyama-P and Tomiyama-SC are almost similar, and those of Tomiyama-C and Ishii-Zuber are similar to each other. It can be considered that the bubble is expected to behave according to the value of the drag coefficient obtained by the correlation between Tomiyama-P and Ishii-Zuber.

### 2.3. Interface coupling

The unresolved approach was used to couple the two Lagrangian methods. The resolved approach interprets the continuous phase (liquid) using a length scale that is much smaller than that of the dispersed phases, such as a bubble, which computes the interaction between the two phases using very detailed information of flow around the bubble.

On the other hand, the unresolved approach adopts a length scale of almost similar size in the continuous and dispersed phases, and an empirical closure correlation is used for the mutually transmitted force between the two phases. This approach is suitable for analyzing the interaction behavior of numerous bubbles in a larger area. The unresolved approach uses the Navier-Stokes equation with the local averaging technique for the analysis of the continuous phase and does not consider the collision between the liquid and bubble particles.

The governing equation for the liquid phase using the local averaging technique [47] is as follows:

$$\frac{D(\varepsilon\rho_L)}{Dt}+\nabla\cdot\left(\varepsilon\rho_L\vec{u}_L\right)=0 \tag{32}$$

$$\rho_L\frac{D\left(\varepsilon\vec{u}_L\right)}{Dt}=-\varepsilon\nabla p+\mu_L\nabla\cdot\left(\varepsilon\nabla\vec{u}_L\right)+\varepsilon\rho_L\vec{g}-\vec{f}_B \tag{33}$$

Here, $\varepsilon$ is the volume fraction of the liquid, and $\vec{f}_B$ is the interaction force transferred to the liquid by the bubble. The behavior of the bubble

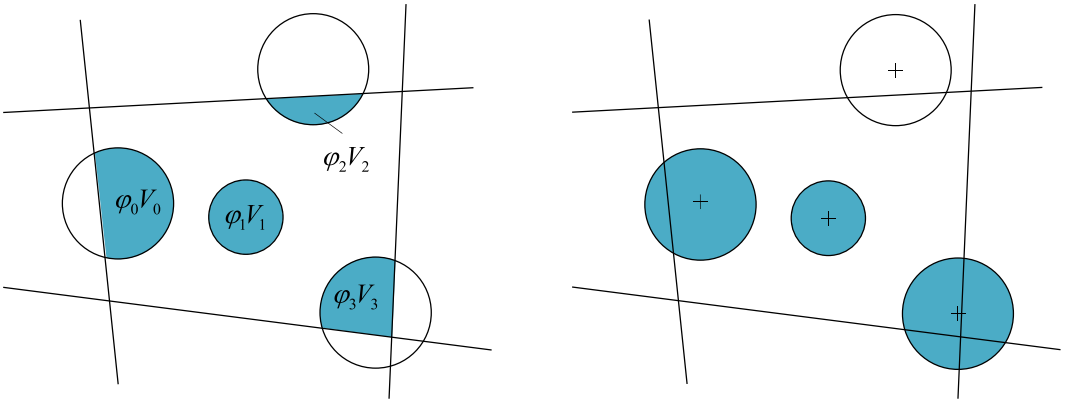


**Fig. 4.** Estimation of liquid volume fraction.

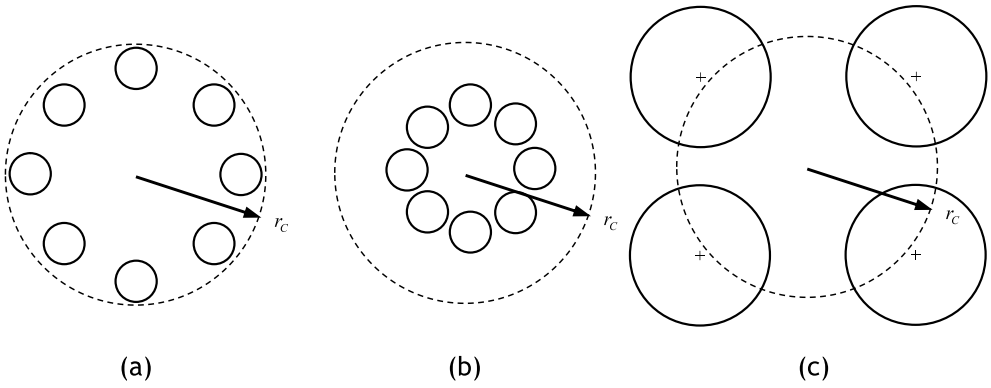


**Fig. 5.** Examples of cases involving errors in estimating the volume fraction.

inside the liquid is influenced by the forces listed in Eq. (13), and the corresponding momentum is transmitted to the liquid according to Newton's 3rd law of motion.

Zhou et al. [48] compared the difference of the methods of processing the pressure term of the momentum equation and the liquid stress tensor in the coupling analysis with solid particles existing in the liquid. In this study, the method specified as Set II in Zhou et al. [48] is used, and in this method, the two phases share the pressure and liquid stress tensor, which can be summarized as follows.

$$\rho_L \frac{D\left(\varepsilon \vec{u}_L\right)}{Dt} = -\nabla p + \nabla \cdot \tau_L + \varepsilon \rho_L \vec{g} - \vec{\Phi} \tag{34}$$

$$\vec{\Phi} = \frac{1}{\Delta V}\left(-V_B \nabla p + V_B \nabla \cdot \tau_L\right) + \vec{f}_B \tag{35}$$

Here, $\vec{\Phi}$ is the force transferred from the bubble to the liquid, the 2nd term on the right in Eq. (35) is the viscous force due to the liquid shear stress, and $\Delta V$ is the constant volume inside the space, $\vec{f}_B$ represents other external forces acting on the bubble existing inside $\Delta V$. Considering Eq. (35), when rewriting Eq. (34), the same expression as that in Eq. (33) is obtained.

### 2.4. Volume fraction

In this study, we propose a rigorous method to accurately estimate the volume fraction. Therefore, it is necessary to calculate the interfacial force accurately.

In Eulerian analysis using a grid system, the volume fraction of liquid is defined as follows (See Fig. 4):

$$\varepsilon_i = 1 - \frac{\sum_j \varphi_j V_j}{\Delta V_i} \tag{36}$$

To estimate the volume fraction in the fully Lagrangian approach (MPS-DEM), Yamada and Sakai [28] defined the volume fraction of liquid as follows:

$$\varepsilon_i = 1 - \frac{\sum_j V_{B_j} w^C\left(\left|\vec{r}_{ij}\right|\right)}{\int w^C(|\vec{r}|)dr} \tag{37}$$

They also used the following weighting function to find the volume fraction.

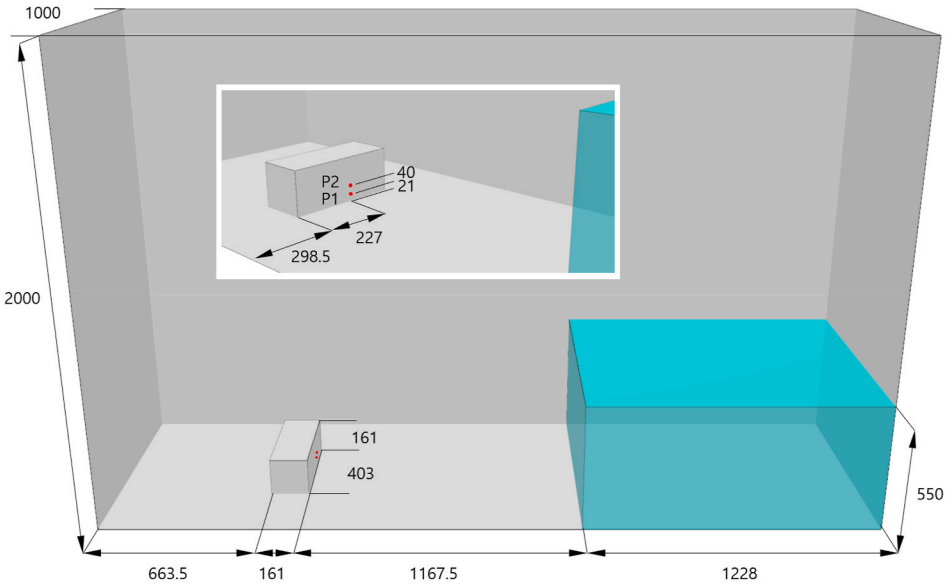


**Fig. 6.** The schematic of the simulation domain (Dam break with an obstacle).

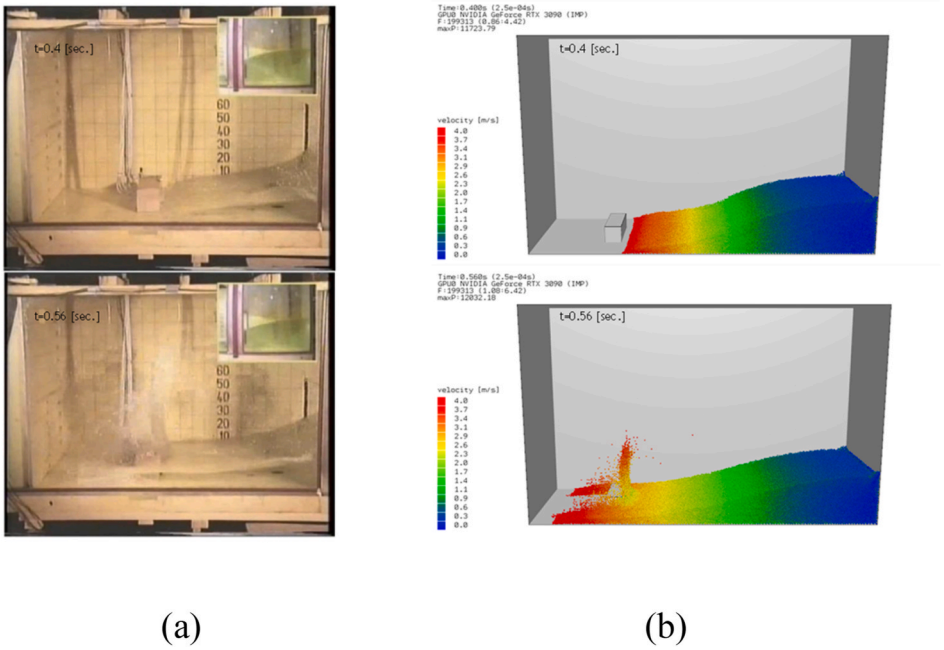


**Fig. 7.** Comparison of the snapshots (a) experiment (b) simulation at t = 0.4 s and 0.56 s.

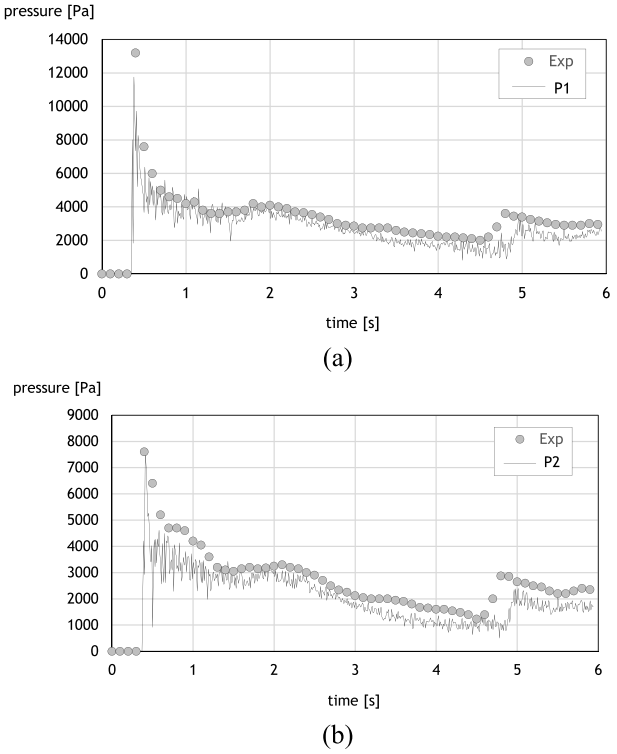


**Fig. 8.** Time histories of pressure (a) P1 (b) P2.

$$w^C\left(\left|\vec{r}_{ij}\right|\right) = \begin{cases} 4\left(\frac{\left|\vec{r}_{ij}\right|}{r_C}\right)^5 - 5\left(\frac{\left|\vec{r}_{ij}\right|}{r_C}\right)^4 + 1 & \left|\vec{r}_{ij}\right| < r_C \\ 0 & r_C \le \left|\vec{r}_{ij}\right| \end{cases} \tag{38}$$

Fig. 5 shows the error that occurs when calculating the volume fraction using Eq. (37). As shown in Fig. 5 (a) and 5 (b), the volume fraction calculated using Eq. (37) has different values depending on the distance-based kernel function. Fig. 5 (c) shows the PCM error due to the bubble's center point being outside the coupling radius $r_C$.

In this study, a rigorous method is used to estimate the volume fraction in the Lagrangian method. The volume, defined as the overlap between the virtual sphere defined by the coupling radius $r_C$ and the arbitrary bubble, is a sphere-sphere intersection. If the distance between the centers of these two spheres is $d$ and the radius of the bubble is $r$, the intersection volume between them is as follows:

$$V_{\text{int}} = \frac{\pi}{12d}\{(r_C + r) - d\}^2\left[d\{d + 2(r_C + r)\} - 3(r_C - r)^2\right] \quad (0 < d) \tag{39}$$

To avoid the error shown in Fig. 5 (c), it is suggested to use a radius larger than the coupling radius as the radius of the bubble to search for surrounding bubbles. In actual calculations, it is inefficient to search for bubbles within the coupling radius for all MPS particles in the liquid, and to calculate the liquid volume fraction by applying Eq. (36). Therefore, in this study, interpolation was performed by creating a lookup table with pre-calculated results for two dimensionless numbers defined as the ratio of the coupling radius to the radius of the bubble and the ratio of the distance ($d$) to the coupling radius.

## 3. Validation

### 3.1. Dam break with an obstacle

To validate the MPS implemented for the liquid phase, we compared the results of the experiments conducted by Kleefsman et al. [49]. This experimental result was used to verify the MPS solver proposed by Zhang [30]. A water tank, of dimensions $3,220 \times 2,000 \times 1,000\ mm^3$ containing a rectangular obstacle of dimensions $161 \times 161 \times 403\ mm^3$ was considered. The initial water column exists in the area of $1,228 \times 550 \times 1,000\ mm^3$, and pressure transducers were installed on the obstacle surface, as shown in Fig. 6, to measure the pressure.

The simulation was performed using 199,313 particles with a particle size of 15 mm. The photographic results were captured through the experiment at t = 0.4 s and 0.56 s and snapshots of the simulation at these instants are presented in Fig. 7 for the purpose of comparison.

In Fig. 8, the pressures measured at P1 and P2 agree well with the overall trend. However, in the case of P2, the pressure was slightly lower

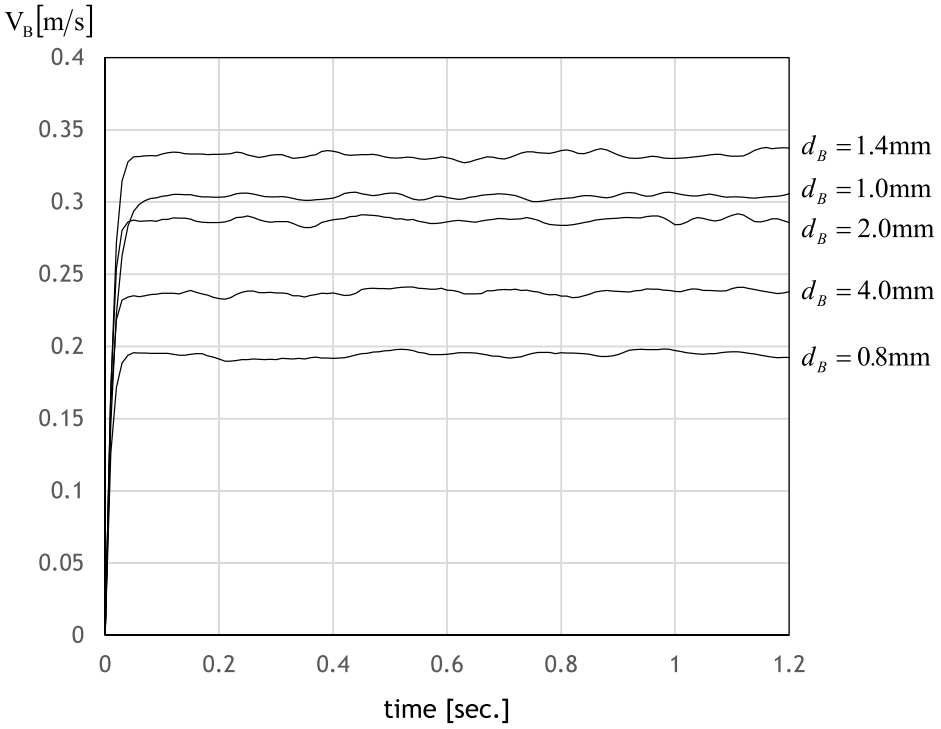


**Fig. 9.** Time histories of single bubble velocity.

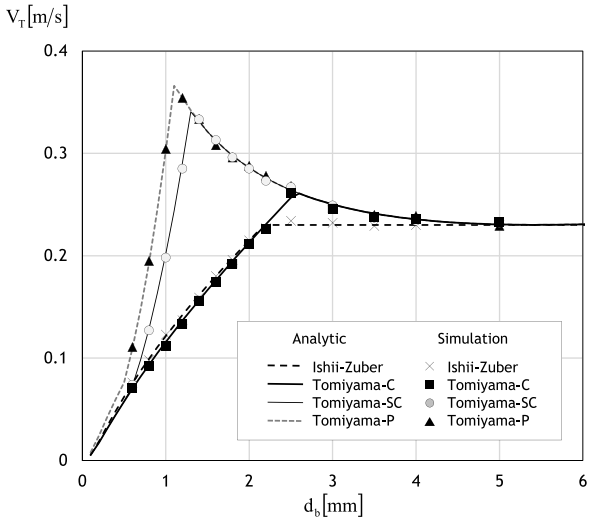


**Fig. 10.** Comparison of the terminal rising velocities of single bubbles.

than that in the experiment. In particular, the pressure at approximately 1 s immediately after the water collides with the obstacles is somewhat different from the experiment. The difference exists between 4.8 s and 5.0 s, which occurs at the instant of the 2nd run-up of a wave against the obstacle. This problem was also observed by Zhang et al. [30].

### 3.2. Terminal rising velocity of a single bubble

The terminal rising velocity of a single bubble obtained by the analytic method from the correlation between the four drag coefficients in Section 2.2, is compared with the analysis result using the coupled MPS-DBM solver developed here. A single bubble with a diameter of 0.6 mm–5 mm is created inside a $150 \times 550 \times 150\ mm^3$ water tank with a square cross section to obtain the terminal rising velocity of the bubble. In this simulation, an MPS particle size of 5 mm and 80,448 particles were used.

As shown in Fig. 9, when the drag correlation in Eq. (19) (Tomiyama-P) is used, the single bubble velocities for bubbles of diameter 0.8, 1.0, 1.4, 2.0, and 4.0 mm are calculated over time. A bubble in the stationary state converges to the terminal rising velocity very quickly.

As shown in Fig. 10, when compared, all the measured values agreed with the analytical results obtained in Section 2.2.

### 3.3. Pressure drop through a packed bed

Owing to friction, a pressure drop occurs as liquid passes through a randomly packed bed of spheres. The pressure drop in these liquids was first noted in 1896 by Darcy when he was observing laminar flow of water through a bed of sand. The Carman-Kozeny equation for pressure drop in laminar flow was formulated in 1937. Ergun [50] presented a general equation for calculating the pressure drop under all flow conditions (laminar and turbulent) using extensive experimental data covering a wide range of particle sizes and shapes.

$$-\frac{\Delta p}{H} = \frac{150\mu_L}{d_p^2}\frac{(1-\varepsilon)^2}{\varepsilon^3}U + \frac{1.75\rho_L}{d_p}\frac{(1-\varepsilon)}{\varepsilon^3}U^2 \tag{40}$$

where H is the bed thickness, $d_p$ is the particle diameter, U is the superficial velocity, and $\varepsilon$ is the liquid volume fraction.

To verify the developed solver and the calculation method for the volume fraction proposed here, a comparison was attempted with the Ergun equation [50]. When many solid particles exist in the liquid, the drag force received by each particle is obtained as follows by considering the voidage function proposed by Di Felice [51] when the drag coefficient of a single particle is $C_D$.

$$\vec{F}_{D,i} = \frac{\rho_L}{2}A\left|\vec{v}_L - \vec{v}_i\right|\left(\vec{v}_L - \vec{v}_i\right)\left\{\hat{f}^d\left(\varepsilon, R_{E,i}\right)\frac{24}{R_{E,i}}\right\}$$

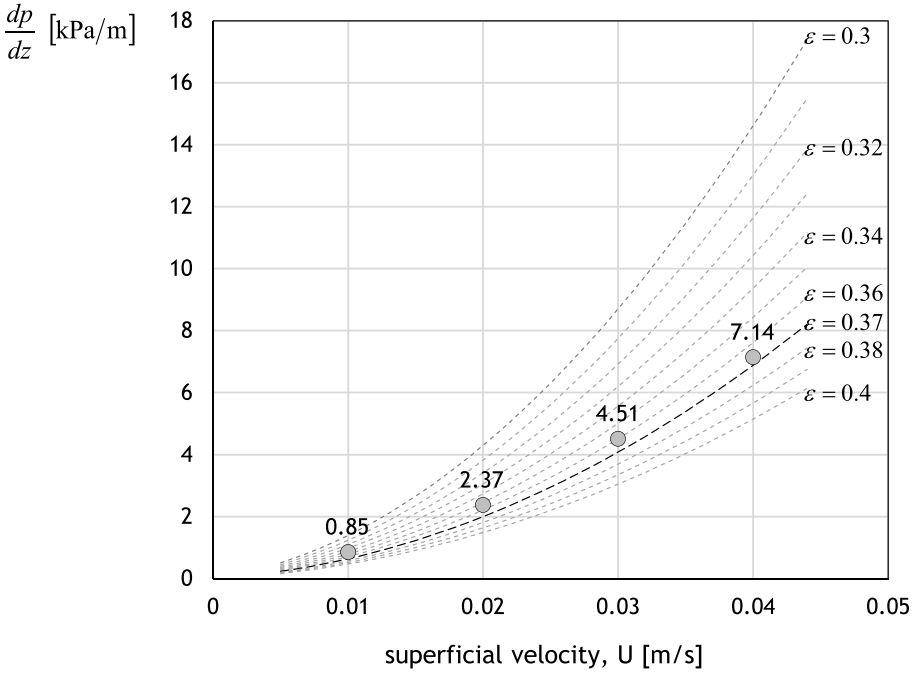


**Fig. 11.** Pressure drop through a packed bed (Ergun equation [50]. vs. simulation).

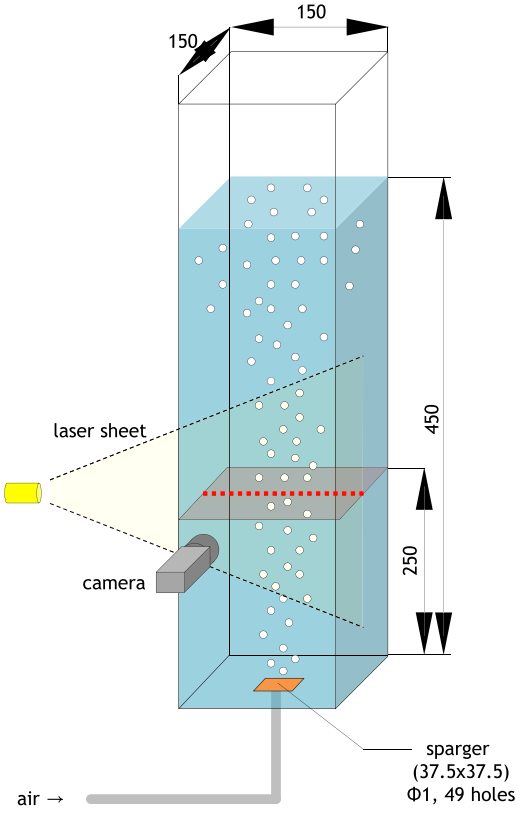


**Fig. 12.** Schematic of the experimental setup [52].

$$R_{E,i}=\frac{\rho_L\left|\vec{v}_L-\vec{v}_i\right|\varepsilon_i d_{p,i}}{\mu_L}$$

$$\widetilde{f}^{d}\left(\varepsilon,R_{E,i}\right)=\frac{C_D}{24}R_{E,i}\varepsilon^{-\chi}$$

$$\chi=3.7-0.65e^{-0.5\left(1.5-log_{10}R_{E,i}\right)^2} \tag{41}$$

The drag force received by each solid particle was calculated using Eq. (41), and the momentum between the two phases was exchanged using the interphase coupling method introduced in Section 2.3. For the simulation, 61,486 particles with particle diameters of 6 mm were randomly stacked in a pipe of diameter 375 mm and length 720 mm to construct a packed bed with a bed height (H) of 100 mm. The volume fraction of the generated packed bed was obtained using Eq. (42)

$$\varepsilon=1-\frac{V_p}{V}=1-\frac{N_p\left(\frac{\pi}{6}\right)d_p^3}{\left(\frac{\pi}{4}\right)D^2L}\sim 0.3704 \tag{42}$$

In this study, the superficial velocity was set in the range of 10 mm/s to 40 mm/s, using an MPS particle size of 6 mm and 349,979 particles. In Fig. 11, the Ergun equation [50] illustrated by Equation (40) is plotted according to the liquid volume fraction $\varepsilon$, and the simulation results are compared on the basis of the superficial velocity U. According to the Ergun equation [50], the pressure drop is very sensitive to the liquid volume fraction. The difference in pressure drop for volume fractions 0.3 and 0.4 is considered to be approximately 10 kPa. It can be seen that it is important to obtain an accurate volume fraction.

## 4. Results

Deen et al. [52] measured the flow of a bubble column in a 150 × 150 × 1000 $mm^3$ square cross-section water tank using particle image velocimetry and laser doppler velocimetry. In this study, 4 g of common salt was added per liter distilled water for a non-coalescing system and filled the tank up to 450 mm (L/D = 3). Air is introduced into the system through a perforated plate that contains 49 holes, each of diameter 1 mm, with a square pitch of 6.25 mm. The bubble column was operated at a superficial velocity of 5 mm/s. The bubble size was approximately 4 mm in this experiment, and the flow velocity was measured in the

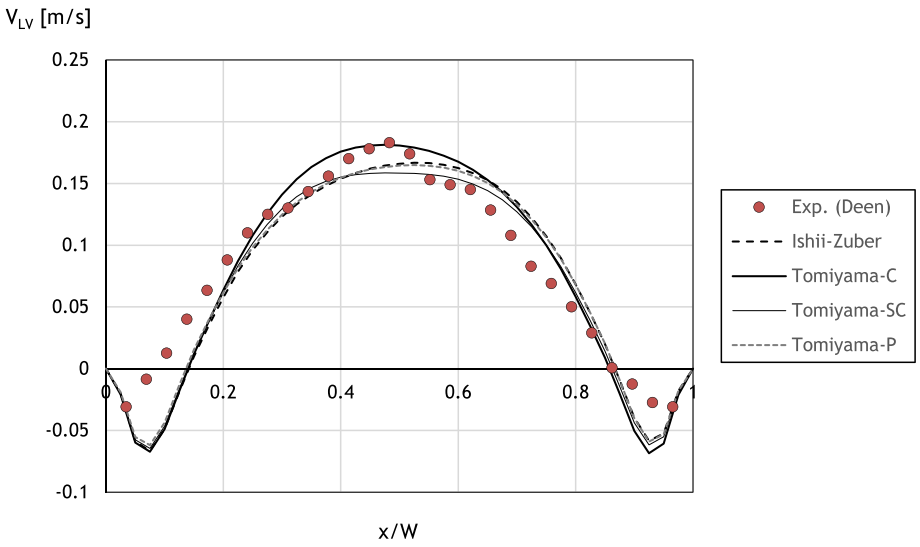


**Fig. 13.** Comparison of mean vertical liquid velocity.

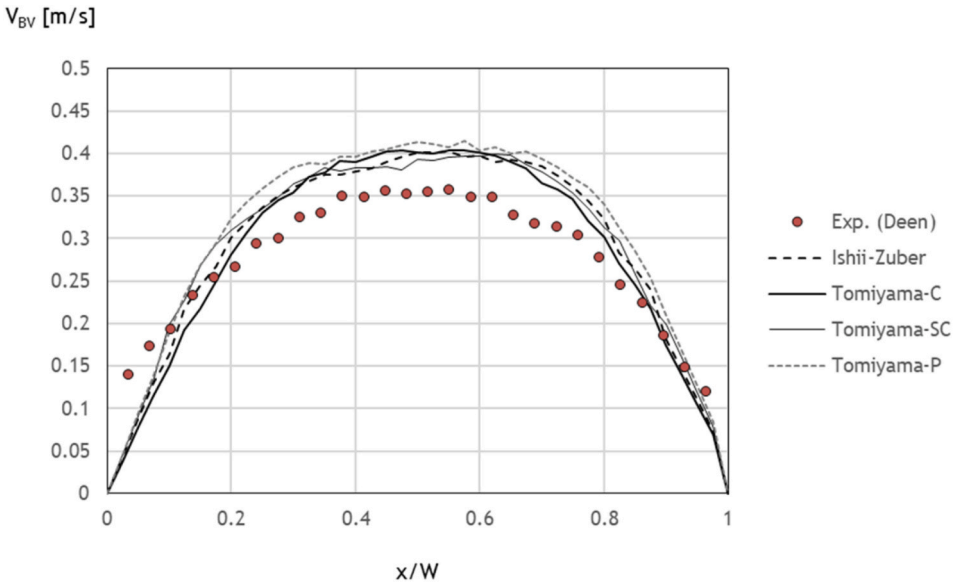


**Fig. 14.** Comparison of mean vertical bubble velocity.

segment defined from one wall to the opposite wall at the center of the plane with Z = 250 mm, as shown in Fig. 12. The experiment proposed by Deen et at [52]. was used for verification of the analysis results in combination with the CFD solver and the DBM proposed in several studies [12–14,17,32,52].

For the simulation, a seed point that could generate a bubble at the bottom was defined, and the bubble was created under the conditions of mean diameter 4 mm and standard deviation 0.5 mm. To satisfy the superficial velocity condition, the inlet boundary condition was implemented on the sparger region of 37.5 × 37.5. For the analysis, 80,448 MPS particles of $l_0 = 5$ mm were used, and the time step was set to approximately $8.3 \times 10^{-5}$ s. To model the water tank, 8,627 nodes and 17,250 triangular elements with an average size of 5 mm were used.

For comparison with the measurement results obtained by Deen et al. [52], a virtual probe that could measure speed at the same point was employed, and the simulation was conducted up to a total of 300 s and the values were statistically processed after 30 s. All the calculations were performed on an Nvidia RTX 3090. This model consists of 24 GB of total dedicated memory and 10,496 CUDA cores.

Fig. 13 illustrates the comparison between the mean vertical velocities of the liquid obtained using the four drag correlations from Eq. (26)–(29). In the case of Tomiyama-SC and Tomiyama-C, the mean vertical velocities of the liquid shows symmetrical profiles, and the maximum velocity is located in the center of the column. In contrast, the Ishii-Zuber and Tomiyama-P cases show not only a slightly asymmetrical profile, but also a slightly biased maximum velocity. Overall, the analysis followed the characteristics determined by the experiment well; however, there was a slight difference in some areas at both ends (near the wall). No significant difference was found in any of the four drag correlations except for some central regions of Tomiyama-C, and the differences between these correlations were negligible. As seen in Fig. 14, the comparison of the simulated mean bubble velocity profile with experimental data is overestimated in all drag correlations. In particular, there are large differences in the bubble velocity compared to the liquid velocity profile at the center of the column. We assume that the difference in bubble velocity compared with that obtained from the experiment is caused by the absence of closures about the bubble size and shape, because the wobbling motion of the bubbles cannot be

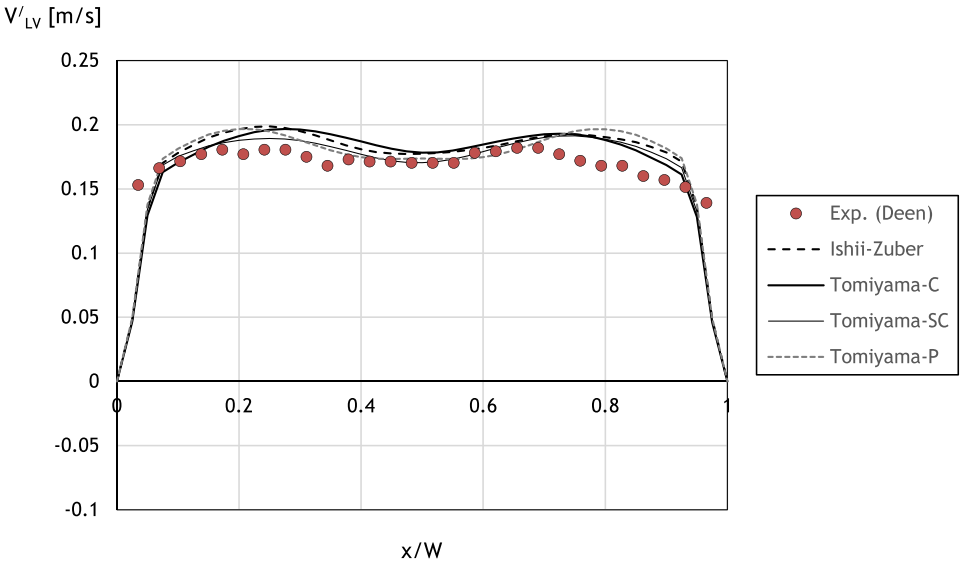


**Fig. 15.** Comparison of mean vertical liquid velocity fluctuation.

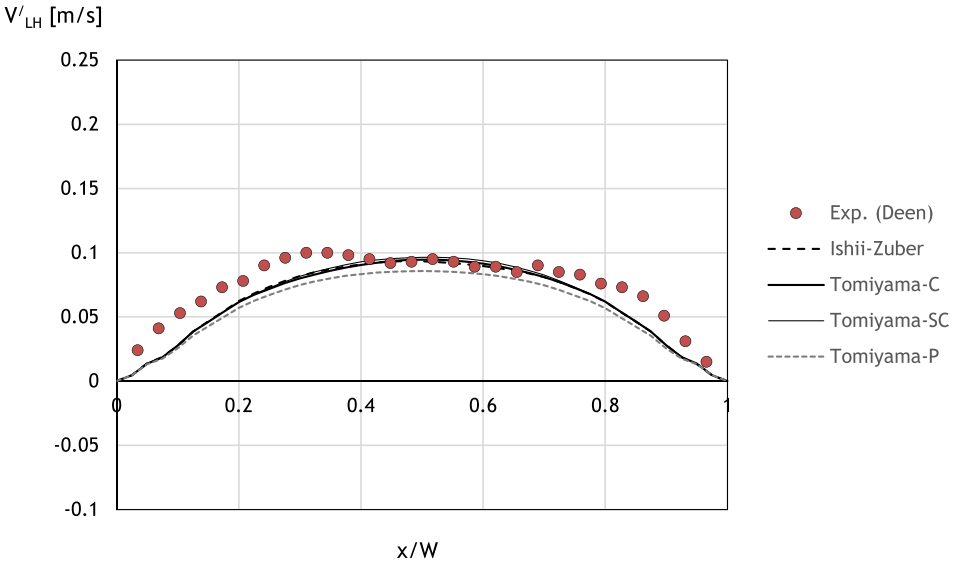


**Fig. 16.** Comparison of mean horizontal liquid velocity fluctuation.

implemented using fixed shapes and sizes of the bubbles.

As seen in Fig. 15, the simulated and experimental mean vertical velocity fluctuations of the liquid are well-matched. All profiles are weakly overestimated in the acceptable range. However, the vertical fluctuation profile in the column center did not differ between Tomiyama-P and Tomiyama-C. Likewise, the simulated mean liquid horizontal velocity fluctuation profiles agree with the experimental results in Fig. 16. Compared to the experimental profiles, the simulated profiles show a weak underestimation in the acceptable range. In the horizontal fluctuation, the simulated profiles are almost the same as the experimental profiles by Ishii-Zuber, Tomiyama-SC, and Tomiyama-C in the column center. Similar to the case of mean velocity, the absence of closures about the bubble size and shape causes the vertical fluctuation of liquid velocity to be overestimated and the horizontal fluctuation of liquid velocity to be underestimated.

## 5. Conclusion

To prevent the release of radioactive material in the case of a severe accident, it is important to understand bubble-induced flow. In this study, we introduced the fully Lagrangian approach to simulate a high gas holdup bubble flow. As the dispersed phases are modeled by a Lagrangian method, there is no need to apply additional techniques to trace the bubble interfaces and describe the interaction between bubble and bubble and bubble-liquid. Likewise, the continuous phases modeled by the Lagrangian method can naturally implement the dynamic motion of the free surface while satisfying volume conservation. These two Lagrangian methods were combined with unresolved approaches and used to successfully simulate a high gas holdup bubble column. The proposed fully Lagrangian method can simulate bubble-induced flows without the disadvantages of the Eulerian approach, such as mesh dependency and difficulties in implementing deformable free surfaces and interfaces.

For an accurate calculation of the momentum transfer between the bubble and liquid, it is necessary to estimate the exact volume fraction at each particle position. In this study, we introduced the error that occurs when calculating the volume fraction using a generally used distance-based kernel and proposed a rigorous method to estimate the exact volume fraction. The proposed method is used for the analytical calculation of the overlapping volume between a virtual sphere defined by the coupling radius and a bubble with an arbitrary size; it can be used to obtain the exact volume fraction. This method of estimating the volume fraction was verified by comparing it with the Ergun equation for determining the pressure drop through a packed bed.

The bubble column flows were simulated for the four correlations of the drag force, in which the effect of the shape and size of the bubble was considered in the experiment. Each numerical result, which depends on the correlations, showed quantitative agreement with the experimental results, and the differences in the results according to the drag correlation were very small. This can be explained through comparisons of the terminal rising velocity and drag coefficient. Consequently, we confirmed that the presented method can successfully simulate bubble-induced flows with a high gas holdup and free surface, which is necessary for various industries, especially for the purpose of nuclear safety.

In the present work, increase of bubble size, coalescence and breakup were not considered. It is necessary to implement this phenomenon for accurate comparison with experimental results such as the void fraction. This will be implemented in a future work. The bubble-induced turbulence models, which are not adopted in this study, will improve the accuracy of the results.

## Declaration of competing interest

The authors declare that they have no known competing financial interests or personal relationships that could have appeared to influence the work reported in this paper.

## References


[1] E. Kim, W.H. Jung, J.H. Park, H.S. Park, K. Moriyama, Experiments on sedimentation of particles in a water pool with gas inflow, Nucl. Eng. Technol. 48 (2016), https://doi.org/10.1016/j.net.2015.12.007.

[2] Y.B. Jo, S. Park, E.S. Kim, Numerical simulation of 3-phase debris bed hydrodynamic leveling behavior using multi-phase SPH-DEM coupling, in: *Transactions Of the Korean Nuclear Society Virtual Spring Meeting,* Online, 2020. July 9-10.

[3] S. Yakush, P. Kudinov, Simulation of ex-vessel debris bed formation and coolability in a LWR severe accident, in: Proceedings of ISAMM-2009, Böttstein, Switzerland, 2009. Oct 25-28.

[4] E.S. Kim, S.H. Park, Y.B. Jo, Status of particle-based multi-physics simulation for nuclear severe accident: review, in: *Transactions Of the Korean Nuclear Society Virtual Spring Meeting,* Online, May 13-14, 2021.

[5] S.H. Park, Y.B. Jo, Y. Ahn, H.Y. Choi, T.S. Choi, S.S. Park, H.S. Yoo, J.W. Kim, E. S. Kim, Development of multi-GPU–based smoothed particle hydrodynamics code for nuclear thermal hydraulics and safety: potential and challenges, Front. Energy Res. (2020) 8, https://doi.org/10.3389/fenrg.2020.00086.

[6] Y.B. Jo, S.H. Park, H.S. Yoo, E.S. Kim, GPU-based SPH-DEM method to examine the three-phase hydrodynamic interactions between multiphase flow and solid particles, Int. J. Multiphas. Flow (2022) 153, https://doi.org/10.1016/j.ijmultiphaseflow.2022.104125.

[7] E. Kim, M. Lee, H.S. Park, K. Moriyama, J.H. Park, Development of an ex-vessel corium debris bed with two-phase natural convection in a flooded cavity, Nucl. Eng. Des. 298 (2016), https://doi.org/10.1016/j.nucengdes.2015.12.028.

[8] A. Konovalenko, S. Basso, P. Kudinov, S.E. Yakush, Experimental investigation of particulate debris spreading in a pool, Nucl. Eng. Des. 297 (2016), https://doi.org/10.1016/j.nucengdes.2015.11.039.

[9] D. Jain, J.A.M. Kuipers, N.G. Deen, Numerical study of coalescence and breakup in a bubble column using a hybrid volume of fluid and discrete bubble model approach, Chem. Eng. Sci. 119 (2014), https://doi.org/10.1016/j.ces.2014.08.026.

[10] M. Van Sint Annaland, N.G. Deen, J.A.M. Kuipers, Numerical simulation of gas bubbles behaviour using a three-dimensional volume of fluid method, Chem. Eng. Sci. 60 (2005), https://doi.org/10.1016/j.ces.2005.01.031.

[11] R.F.L. Cerqueira, E.E. Paladino, F. Evrard, F. Denner, B. Wachem, van Multiscale modeling and validation of the flow around taylor bubbles surrounded with small dispersed bubbles using a coupled VOF-DBM approach, Int. J. Multiphas. Flow (2021) 141, https://doi.org/10.1016/j.ijmultiphaseflow.2021.103673.

[12] D. Darmana, N.G. Deen, J.A.M. Kuipers, Detailed modeling of hydrodynamics, mass transfer and chemical reactions in a bubble column using a discrete bubble model, Chem. Eng. Sci. 60 (2005) 3383–3404, https://doi.org/10.1016/J.CES.2005.01.025.

[13] D. Darmana, R.L.B. Henket, N.G. Deen, J.A.M. Kuipers, Detailed modelling of hydrodynamics, mass transfer and chemical reactions in a bubble column using a discrete bubble model: chemisorption of CO2 into NaOH solution, numerical and experimental study, Chem. Eng. Sci. 62 (2007), https://doi.org/10.1016/j.ces.2007.01.065.

[14] D. Jain, Y.M. Lau, J.A.M. Kuipers, N.G. Deen, Discrete bubble modeling for a micro-structured bubble column, Chem. Eng. Sci. 100 (2013), https://doi.org/10.1016/j.ces.2013.02.060.

[15] J.B. Joshi, Computational flow modelling and design of bubble column reactors, Chem. Eng. Sci. 56 (2001).

[16] G.R. Guédon, G. Besagni, F. Inzoli, Prediction of gas–liquid flow in an annular gap bubble column using a Bi-dispersed eulerian model, Chem. Eng. Sci. 161 (2017), https://doi.org/10.1016/j.ces.2016.12.015.

[17] A. Asad, C. Kratzsch, R. Schwarze, Influence of drag closures and inlet conditions on bubble dynamics and flow behavior inside a bubble column, Eng. Appl. Comput. Fluid Mech. 11 (2017), https://doi.org/10.1080/19942060.2016.1249410.

[18] X. Sun, M. Sakai, Y. Yamada, Three-dimensional simulation of a solid-liquid flow by the DEM-SPH method, J. Comput. Phys. 248 (2013), https://doi.org/10.1016/j.jcp.2013.04.019.

[19] M. Robinson, M. Ramaioli, S. Luding, Fluid-particle flow simulations using two-way-coupled mesoscale SPH-DEM and validation, Int. J. Multiphas. Flow 59 (2014), https://doi.org/10.1016/j.ijmultiphaseflow.2013.11.003.

[20] S.J. Neethling, D.J. Barker, Using smooth particle hydrodynamics (SPH) to model multiphase mineral processing systems, Miner. Eng. 90 (2016), https://doi.org/10.1016/j.mineng.2015.09.022.

[21] E. Harada, H. Gotoh, H. Ikari, A. Khayyer, Numerical simulation for sediment transport using MPS-DEM coupling model, Adv. Water Resour. 129 (2019), https://doi.org/10.1016/j.advwatres.2017.08.007.

[22] E. Harada, T. Tazaki, H. Gotoh, Numerical investigation of ripple in oscillating water tank by DEM-MPS coupled solid–liquid two-phase flow model, J.Hydro-Environ. Res. (2020) 32, https://doi.org/10.1016/j.jher.2020.07.001.

[23] E. Harada, H. Ikari, T. Tazaki, H. Gotoh, Numerical simulation for coastal morphodynamics using DEM-MPS method, Appl. Ocean Res. 117 (2021), https://doi.org/10.1016/j.apor.2021.102905.

[24] T. Tazaki, E. Harada, H. Gotoh, Vertical sorting process in oscillating water tank using DEM-MPS coupling model, Coast Eng. (2021) 165, https://doi.org/10.1016/j.coastaleng.2020.103765.

[25] S. Koshizuka, Y. Oka, Moving-particle semi-implicit method for fragmentation of incompressible fluid, Nucl. Sci. Eng. 123 (1996), https://doi.org/10.13182/NSE96-A24205.

[26] S. Koshizuka, A. Nobe, Y. Oka, Numerical analysis of breaking waves using the moving particle semi-implicit method, Int. J. Numer. Methods Fluid. 26 (1998), https://doi.org/10.1002/(sici)1097-0363(19980415)26:7<751::aid-fld671>3.0.co;2-c.

[27] S. Koshizuka, H. Ikeda, Y. Oka, Numerical analysis of fragmentation mechanisms in vapor explosions, Nucl. Eng. Des. 189 (1999) 423–433, https://doi.org/10.1016/S0029-5493(98)00270-2.

[28] Y. Yamada, M. Sakai, Lagrangian-Lagrangian simulations of solid-liquid flows in a bead mill, Powder Technol. 239 (2013), https://doi.org/10.1016/j.powtec.2013.01.030.

[29] G. Duan, S. Koshizuka, A. Yamaji, B. Chen, X. Li, T. Tamai, An accurate and stable multiphase moving particle semi-implicit method based on a corrective matrix for all particle interaction models, Int. J. Numer. Methods Eng. 115 (2018) 1287–1314, https://doi.org/10.1002/nme.5844.

[30] T. Zhang, S. Koshizuka, P. Xuan, J. Li, C. Gong, Enhancement of stabilization of MPS to arbitrary geometries with a generic wall boundary condition, Comput. Fluids 178 (2019) 88–112, https://doi.org/10.1016/J.COMPFLUID.2018.09.008.

[31] M.A. Basit, W. Tian, R. Chen, R. Basit, S. Qiu, G. Su, Investigation of single bubble behavior under rolling motions using multiphase MPS method on GPU, Nucl. Eng. Technol. (2021) 53, https://doi.org/10.1016/j.net.2020.12.013.

[32] J. Ma, G.L. Chahine, C.T. Hsiao, Spherical bubble dynamics in a bubbly medium using an euler-Lagrange model, Chem. Eng. Sci. 128 (2015), https://doi.org/10.1016/j.ces.2015.01.056.

[33] T. Ziegenhein, R. Rzehak, E. Krepper, D. Lucas, Numerical simulation of polydispersed flow in bubble columns with the inhomogeneous multi-size-group model, Chem. Ing. Tech. 85 (2013), https://doi.org/10.1002/cite.201200223.

[34] D. Lucas, R. Rzehak, E. Krepper, T. Ziegenhein, Y. Liao, S. Kriebitzsch, P. Apanasevich, A strategy for the qualification of multi-fluid approaches for nuclear reactor safety, in: Proceedings of the Nuclear Engineering and Design vol. 299, 2016.

[35] R. Rzehak, M. Krauß, P. Kováts, K. Zähringer, Fluid dynamics in a bubble column: new experiments and simulations, Int. J. Multiphas. Flow 89 (2017), https://doi.org/10.1016/j.ijmultiphaseflow.2016.09.024.

[36] E.I.V. Van Den Hengel, N.G. Deen, J.A.M. Kuipers, Application of coalescence and breakup models in a discrete bubble model for bubble columns, Ind. Eng. Chem. Res. 44 (2005), https://doi.org/10.1021/ie0492449.

[37] S.H. Park, Y.B. Jo, Y. Ahn, H.Y. Choi, T.S. Choi, S.S. Park, H.S. Yoo, J.W. Kim, E. S. Kim, Development of multi-GPU–based smoothed particle hydrodynamics code for nuclear thermal hydraulics and safety: potential and challenges, Front. Energy Res. (2020) 8, https://doi.org/10.3389/fenrg.2020.00086.

[38] H. Gotoh, T. Sakai, T. Shibahara, Lagrangian flow simulation with SUB-PARTICLE-SCALE turbulence model, Proc. Hydraul. Eng. 44 (2000), https://doi.org/10.2208/prohe.44.575.

[39] J. Arai, S. Koshizuka, K. Murozono, Large eddy simulation and a simple wall model for turbulent flow calculation by a particle method, Int. J. Numer. Methods Fluid. 71 (2013), https://doi.org/10.1002/fld.3685.
[40] E. Delnoij, J.A.M. Kuipers, W.P.M. van Swaaij, A three-dimensional CFD model for gas–liquid bubble columns, Chem. Eng. Sci. 54 (1999) 2217–2226, https://doi.org/10.1016/S0009-2509(98)00362-5.
[41] H. Rusche, Computational Fluid Dynamics of Dispersed Two-phase Flows at High Phase Fractions, PhD Thesis, Imperial College London (University of London), 2002.
[42] A. Tomiyama, H. Tamai, I. Zun, S. Hosokawa, Transverse migration of single bubbles in simple shear flows, Chem. Eng. Sci. 57 (2002) 1849–1858, https://doi.org/10.1016/S0009-2509(02)00085-4.
[43] S. Hosokawa, A. Tomiyama, S. Misaki, T. Hamada, Lateral migration of single bubbles due to the presence of wall, in: Proceedings of the American Society of Mechanical Engineers vol. 257, Fluids Engineering Division (Publication) FED, 2002.
[44] R. Rzehak, E. Krepper, C. Lifante, Comparative study of wall-force models for the simulation of bubbly flows, Nucl. Eng. Des. 253 (2012), https://doi.org/10.1016/j.nucengdes.2012.07.009.
[45] A.D. Burns, T. Frank, I. Hamill, J.M. Shi, The Favre Averaged Drag Model for Turbulent Dispersion in Eulerian Multi-phase Flows, 5th International Conference on Multiphase Flow, Yokohama, Japan, 2004. May 30 - June 4.
[46] Y. Tsuji, T. Tanaka, T. Ishida, Lagrangian numerical simulation of plug flow of cohesionless particles in a horizontal pipe, Powder Technol. 71 (1992), https://doi.org/10.1016/0032-5910(92)88030-L.
[47] T.B. Anderson, R.O.Y. Jackson, A fluid mechanical description of fluidized beds, Ind. Eng. Chem. Fundam. 6 (1967).
[48] Z.Y. Zhou, S.B. Kuang, K.W. Chu, A.B. Yu, Discrete particle simulation of particle-fluid flow: model formulations and their applicability, J. Fluid Mech. 661 (2010), https://doi.org/10.1017/S002211201000306X.
[49] K.M.T. Kleefsman, G. Fekken, A.E.P. Veldman, B. Iwanowski, B. Buchner, A volume-of-fluid based simulation method for wave impact problems, J. Comput. Phys. (2005) 206, https://doi.org/10.1016/j.jcp.2004.12.007.
[50] S. Ergun, Fluid flow through packed columns, Chem. Eng. Prog. 48 (1952) citeulike-article-id:7797897.
[51] R. di Felice, The voidage function for fluid-particle interaction systems, Int. J. Multiphas. Flow 20 (1994), https://doi.org/10.1016/0301-9322(94)90011-6.
[52] N.G. Deen, T. Solberg, B.H. Hjertager, Large eddy simulation of the gas-liquid flow in a square cross-sectioned bubble column, Chem. Eng. Sci. 56 (2001), https://doi.org/10.1016/S0009-2509(01)00249-4.